Cloud cavitation vortex shedding inside an injector nozzle

N. Mitroglou[1], V. Stamboliyski[2], I. K. Karathanassis[1,*], K. S. Nikas[2] and M. Gavaises[1]

[1]*School of Mathematics Computer Science and Engineering, City, University of London, London, EC1V 0HB, UK*

[2]*Technological Education Institute of Piraeus, Piraeus, 122 41, Greece*

[*] *Corresponding author: Ioannis.Karathanassis@city.ac.uk*

Abstract. The development and collapse of cloud cavitation and its link to surface erosion within a transparent test single-orifice nozzle operating with a closed Diesel fuel hydraulic circuit, has been characterized using high-speed imaging. Data have been obtained for a range of cavitation and Reynolds numbers under fixed lift positions. Post processing of a large number of images acquired with short exposure time (1μs) allowed the elucidation of the distinct flow phenomena associated with the highly transient two-phase flow. At the inlet of the flow orifice, the vapour cloud was found to occupy the largest part of the nozzle hole cross-section. Coherent vortical structures of a hairpin shape have been detected to onset at the closure region of this vapour cloud and shed downstream in a fully transient manner. The effect of the operating parameters on the temporal and spatial characteristics with regards to the emergence and collapse of the hairpin vortices has been quantified. It has been established that the cavitation-vortex shedding was taking place in a periodical manner, characterized by a Strouhal number.

Keywords: cloud cavitation, injector flow, high-speed imaging, vapour collapse, erosion

1. INTRODUCTION

Cavitation occurs in a wide range of engineering applications such as marine propellers and rudders, bearings, fuel injectors, pumps and turbines; it is often associated with undesired consequences such as vibration, increased hydrodynamic drag, noise and erosion of solid surfaces. Cavitating flows are unsteady in nature with their distinct flow features exhibiting highly varying spatial topology and short time scales.

Under certain flow conditions, cavitation is possible to exhibit a periodic behavior characterized by the shedding of coherent vortical structures. Vortex shedding has been extensively investigated in non-cavitating flows (see selectively the work of Griffin [1]), as it could lead to flow-induced alterations in the thermal and structural behavior of devices, e.g. heat transfer enhancement, oscillations etc. The influence of the presence of vapour bubbles on the mechanism that induces shedding of coherent vortices has been investigated by a number of researchers [2–4]. Cavitation vortex shedding has been primarily investigated until now in numerous studies relevant to hydrofoil configurations (e.g. propellers, hydrofoils or turbomachinery blades); see selectively the work of Arndt [5] among many other.

A significant number of both experimental-visualization and numerical studies, employing either RANS simulations or LES [2,3,6–15], focus on the interaction of the attached cavitation pocket developing at the leading edge of various hydrofoil shapes (for example twisted [14], elliptical [15] etc) with vortex motion, for different values of the angle of attack and the cavitation index. Huang et al. [12] characterized the prevailing mechanism and described the various phases of cloud cavitation development and vortex shedding taking place at the trailing edge of a benchmark hydrofoil. The coherent vortices that emerge at the hydrofoil trailing edge

and the underlying onset mechanisms have been thoroughly discussed. It has been established that the detachment and periodic shedding of cavitating vortices is associated with the action of a secondary flow motion in the boundary-layer region, commonly termed as re-entrant jet. It is noteworthy to mention that, referring to hydrofoil configurations, vortex shedding frequency has been found to increase in the presence of cavitation [2,3]. A conclusion that can be considered to be valid in other geometrical layouts, according to Sridhar and Katz [16].

A number of primarily experimental studies are available in the open literature, where the distinct flow features characterizing the different cavitation regimes are illustrated in simple layouts with a geometrical constriction. Gopalan and Katz [17] employed PIV visualization and high-speed imaging in order to capture the topology of cavitating flow downstream of a converging nozzle. The value of the cavitation number was properly adjusted to enable the development of sheet cavitation at the nozzle throat. The shedding of three-dimensional, hairpin-shaped vortical structures at the cavitation closure region was detected, although their velocity measurements verified the absence of an upstream flow (re-entrant jet) in the specific area. Instead, the onset of the vortices was attributed to the collapse of vapour bubbles in the region, which acted as a source of localized vorticity. Ganesh et al. [18] used x-ray densitometry to clarify the mechanism that controls cavity-vortex shedding downstream of a two-dimensional wedge layout. Their findings suggest that, depending on the cavitation index, shedding is controlled either by the existence of a re-entrant jet or a bubbly shock wave.

Cavitation in flow orifices has also been studied thoroughly. Stutz and Legupil [19] performed an experimental investigation of the unsteady cavitating flow in a convergent-divergent nozzle with a sharp edge (throat). The authors employed an x-ray technique suitable for measuring instantaneous values of the vapour fraction and verified the detachment of vortical structures from the cavitation cloud downstream of the nozzle tip. The study established that the vortex shedding occurs in a periodical manner with a characteristic frequency corresponding to a Strouhal number value of 0.28. Insight on the transient development of sheet/cloud cavitation is given by the visualization studies supplemented by hybrid RANS/LES simulations performed by Gavaises et al. [20]. The decelerating flow within an axisymmetric throttle realized by two parallel discs was found to lead to the formation of cloud cavitation close to the throttle rounded inlet with subsequent vapour shedding at a Strouhal number in the range 0.2-0.3, depending on the cavitation index. The regions of vapour collapse were found to match well with sites of surface erosion.

Few recent studies have investigated cavitation in fuel injector geometries, typically used with Diesel engines. The studies mainly refer to enlarged replicas of the actual injector geometry, which facilitate the flow visualization and a better spatial resolution can be achieved. For example, the influence of the presence of vortex (string) cavitation inside various nozzle designs on the atomization of the spray has been discussed in detail by Andriotis et al. [21], Mitroglou et al. [22] and Gavaises et al. [23]. These studies justified increase of the spray cone angle of the jet exiting the nozzle and more effective liquid atomization in comparison to flow where strings were absent.

Cavitation in true-scale injectors operating under realistic injection pressures has been also studied, for example see selectively Andriotis et al. [24], Giannadakis et al. [25], Mitroglou et al. [26,27], and Reid et al. [28,29]. Out of those, the study from Reid et al. [28] has been the only one to visualize cavitation at pressures up to 2050 bars. The specific nozzle configuration tested is of particular interest to the present study. Upstream of the three parallel injection holes, a fixed needle was acting as an obstacle to the flow, leading to asymmetric flow inlet. Moreover, it was shown that longitudinal vortices detected as string cavitation formed at the axes of the two parallel holes, whereas an additional cavitating vortex of horseshoe shape was found to “bridge” the two holes. In a subsequent study [29] referring to the same nozzle layout, it was pointed out that the secondary flow topology exhibits significant discrepancies in the

cases of steady state and transient fuel injection conditions. The significance of this study lies on the fact that the same macroscopic flow features that have been observed in transparent nozzles operating at much lower pressures (from a few bar up to 600bar) are present at pressure levels similar to those in real metallic nozzles.

Numerous works have demonstrated that the collapse of cavitation bubbles is responsible for the formation of surface erosion. This is mainly through two mechanisms, namely the pressure wave of considerable magnitude generated by the implosion of bubble clusters and the impingement of micro-jets, which set in during the asymmetric bubble collapse in the vicinity of solid surfaces. The experimental study of Petkovsek and Dular [30] demonstrated that unstable vapour clouds, possibly produced by a shedding mechanism, appear to be more aggressive compared to attached cavities, in terms of erosion induction through a combination of the two mechanisms described above. In a subsequent study, Dular et al. [31] identified the various distinct vortical structures that emanate during the periodical shedding of a vapour cloud and confirmed that the horseshoe-type vortex exhibits the most aggressive behavior in terms of surface erosion. Finally, the pit-count measurements performed by Pelz et al. [32] have shown that the erosion damage caused by cloud cavitation is primarily influenced by the intensity of the cavitation vortices and secondly by the shedding frequency.

The main aim of the present investigation is to elucidate the cavitation phenomena that influence the flow characteristics of fuel-injection systems, which, in turn have a significant effect on the injector structural integrity and the properties of the near-nozzle spray. The major objective of the present investigation is to shed light on the topology and dynamic features of cloud cavitation emanating inside an enlarged, transparent single-orifice fuel injector nozzle. The nozzle configuration has a geometry similar to that investigated by Reid et al. [28] and was installed in a specially designed test bench running under steady-state operating conditions. Despite that, highly transient coherent vapour structures were detected to emerge within the nozzle using high-speed visualization. The collection of images taken at a high frame rate with adequate spatial resolution and over a significant time period allowed the identification of hairpin-shaped cavitating vortices being shed at characteristic frequencies designated by the operating conditions. Furthermore, the locations of onset and collapse of the cavitating cloud have been specified.

The next section offers a brief description of the experimental apparatus employed, followed by the experimental results obtained. The main findings of the study are summarized in the last section.

2. EXPERIMENTAL SETUP

The injector-mimicking arrangement including the custom nozzle flow channel is shown in Fig. 1a. A simplified geometrical layout has been designed, where flow perturbations due to the presence of multiple nozzle holes, typical of common injector arrangements, are absent. The prototype nozzle was manufactured from a transparent acrylic resin, so as to facilitate the unobstructed view of the complex two-phase flow arising inside it, while the nozzle material is capable of withstanding pressures up to 80 bars. As illustrated in Fig. 1b, downstream the flow gallery of 40 mm diameter (see upper part of Fig. 1b) is the main body of the nozzle that features an axisymmetric cylindrical geometry of 10 mm in diameter; at the end of which there is an off-axis injection hole of 3 mm in diameter. Therefore, the 10 mm long flow path is called “sac” and the 3 mm, eccentrically positioned hole of 3 mm is called “injection hole”. A manifold layout precedes the examined nozzle configuration so as to ensure a parallel and unperturbed flow entering the injector. The offset hole placement, along with the asymmetrical needle topology (Fig.1c), produces an asymmetrical flow entering the nozzle hole, which leads to the development of a cavitation pocket mainly on one side of the orifice inlet, thus enabling

full optical access to the cloud cavitation topology from any angle. The working fluid exiting the nozzle is subsequently discharged into a chamber of cubic shape having 50×50mm overall dimensions.

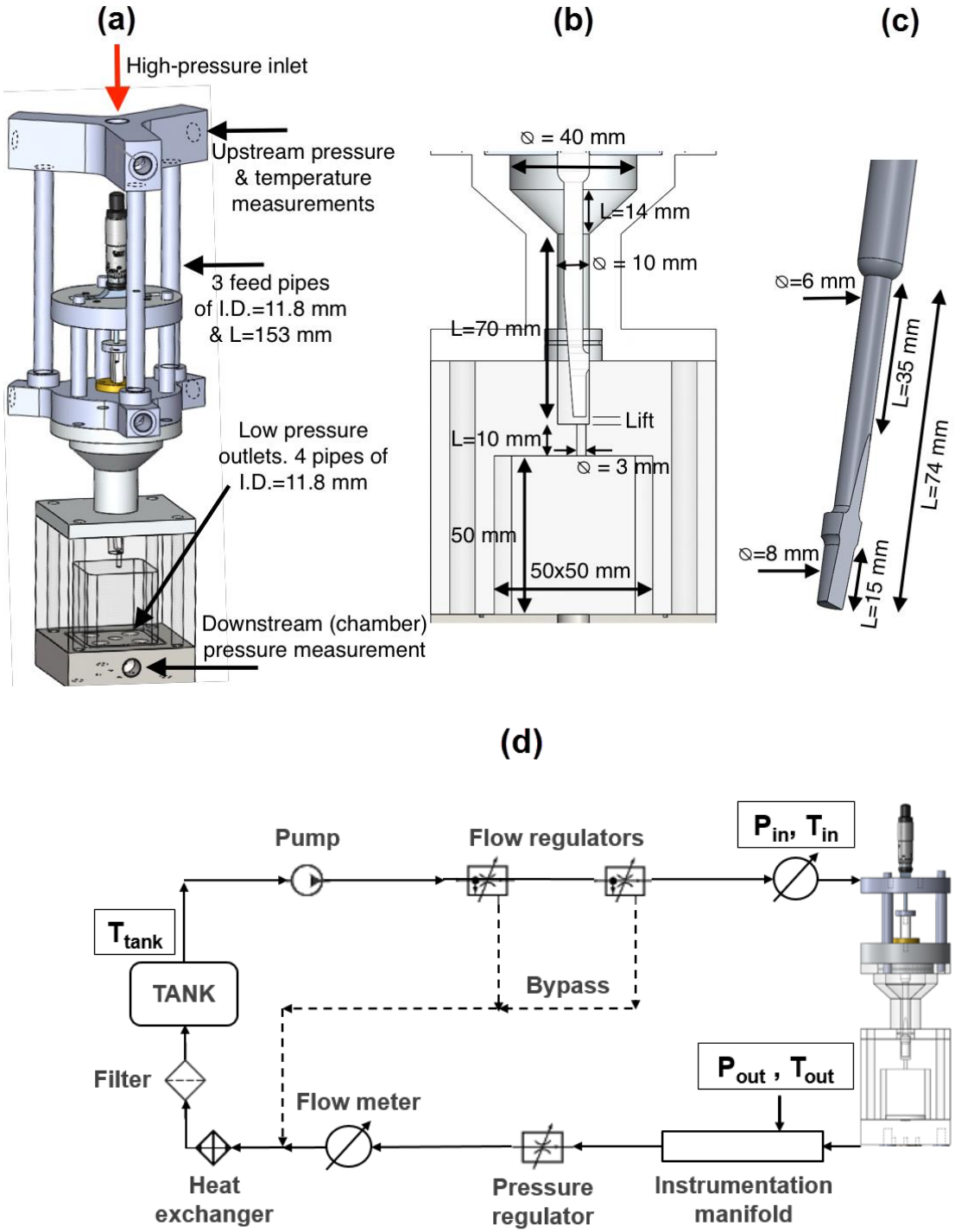

Figure 1. From left to right: (a) Schematic of the test-bench including main instrumentation taps (I.D.: Internal Diameter), (b) cross-sectional detail view of the injector nozzle and discharging chamber, (c) geometrical layout of the needle with main dimensions and (d) schematic of the flow loop.

The hydraulic flow loop that was developed for the present investigation and is depicted on Fig. 1d, was operated at steady-state flow-rate conditions with a commercial Diesel-fuel oil circulating through the model. The liquid thermo-physical properties are in accordance with the EN 590 standard, while its temperature was monitored through type-K thermocouples

inserted at the fuel tank and the inlet manifold and adjusted to a specified set-point with the use of a heat exchanger and a PID controller. Control valves (flow regulators) placed at the outlet of the feed pump were employed for imposing the liquid volumetric flow rate $\dot{V}$, which was monitored through an axial-turbine flow meter. A (nominal) Reynolds number characterizing the flow is defined on basis of the mean flow velocity u_{mean} and the nozzle diameter D:

$$Re = \frac{u_{mean} \cdot D}{\nu_{fuel}} = \frac{4\dot{V}}{(\pi D) \cdot \nu_{fuel}} \quad (1)$$

where ν_{fuel} and $\dot{V}$ are the fuel kinematic viscosity and volumetric flow rate, respectively. Therefore, the Reynolds-number value can be fixed for each case examined, since the fuel temperature is also maintained constant. Flow is expected to exhibit highly transient features with short time scales, as the Reynolds number lies in the range of 50000. Liquid pressure at the inlet and outlet of the test bench was monitored through pressure transducers inserted in taps. For a specified flow rate, the back (chamber) pressure was set to a specific value through a valve located at the outflow manifold downstream the injector outlet, while the upstream pressure adjusted accordingly, so as flow continuity to be satisfied. The cavitation number (CN), indicative of the cavitation-formation intensity, could be subsequently defined as:

$$CN = \frac{p_{inj} - p_{back}}{p_{back} - p_{vap}} \quad (2)$$

where p_{inj}, p_{back} and p_{vap} stand for the injection (upstream), back and vapour pressures, respectively. Based on the error propagation [33] due to the accuracy in the measurement of pressure, velocity and temperature, the uncertainty in the values of the cavitation number are associated with a global uncertainty of 5%.

The different test cases considered in the present evaluation are summarized in Table 1. As can be seen, 14 cases have been included in this study, corresponding to different values of the valve lift, cavitation number and Reynolds numbers. The position of the needle was adjusted by a mechanism seated on the upper part of the test bench, which can be seen on the top part of Fig. 1a, while the fuel thermophysical properties required for the determination of CN were calculated according to the data provided by Kolev [34] and are also reported in Table 1. The Diesel fuel density in the temperature range 320-330K is of the order of 806-812 kg/m^3.

Table 1. Experimental test cases investigated.

Case id.	Lift $\cdot 10^{-3}$ [m]	Re	CN	$\dot{V}$ [l/m]	P_{inj} $\cdot 10^5$ [Pa]	P_{back} $\cdot 10^5$ [Pa]	T_{in} [K]	P_{sat} $\cdot 10^5$ [Pa]	ν_{fuel} $\cdot 10^{-6}$ [m^2/s]
L0.5_CN1.3	0.5	53760	1.3	21.18	41.5	18.2	327.2	0.259	2.19
L0.5_CN1.4			1.4	21.18	40.8	17.1	327.2	0.259	2.19
L0.5_CN1.6			1.6	21.18	40.0	15.6	327.2	0.259	2.19
L0.5_CN1.8			1.8	21.18	39.8	14.4	327.2	0.259	2.19
L0.5_CN2.0			2	21.34	40.2	13.6	326.8	0.257	2.20
L1.0_CN0.9_L	1	53760 (L)	0.9	21.13	36.2	19.2	327.3	0.259	2.18
L1.0_CN1.1_L			1.1	23.11	32.4	15.6	322.6	0.238	2.39
L1.0_CN1.2_L			1.2	23.29	31.2	14.3	322.2	0.236	2.41
L1.0_CN1.3_L			1.3	23.48	30.2	13.3	321.8	0.235	2.43
L1.0_CN1.45_L			1.45	23.57	29.4	12.2	321.6	0.234	2.44
L1.0_CN1.3_H	1	63663 (H)	1.3	23.92	41.3	18.1	329.8	0.272	2.09
L1.0_CN1.45_H			1.45	25.5	40.1	16.5	326.3	0.254	2.23
L2.0_CN1.0	2	53760	1	22.74	28.6	14.4	323.4	0.241	2.35
L2.0_CN1.2			1.2	23.66	26.4	12.2	321.4	0.233	2.44

Shadowgraphy was deemed as a suitable visualization technique for capturing images of the cavitation structures emerging inside the nozzle hole. The experimental setup of the image acquisition methodology is illustrated in Fig. 2; it incorporated a halogen floodlight providing white band light, which was subsequently focused by a Fresnel lens on the area of interest. The placement of a CCD camera in the opposite side of the device allowed for side-view images to be taken of the arising vapour cloud. A high-speed Photron SA1.1 camera was employed, offset to capture 50000 frames per second (fps) at a resolution of 512×208 pixels, was considered to be adequate for elucidating the spatial and temporal development of cavitation. The shutter speed was set at 1μs to increase image clarity and "freeze" the high velocity flow phenomena inside the injection hole. Up to approximately 50000 images were collected for each case examined and thus any flow event occurring in a periodical manner in the nozzle-hole region can be illustrated with clarity. Since the overall length of the visualized hole region is equal to 10 mm and 512 pixels are employed for its discretization, the visualization resolution is equal to 20μm/pixel. The resolution of the visualization technique is in the order of the manufacturing uncertainty associated with the nozzle dimensions, while the size of cloud cavitation and the coherent cavitating vortices is much larger and comparable to the nozzle diameter (equal to 3.0 mm). Hence, the spatial resolution is sufficient for properly illustrating the topology of the two-phase flow within the nozzle. Referring to the temporal resolution, the prevailing occurrence frequency of the periodical flow phenomena taking place within the nozzle was found to lie well within the range detectable using a frame rate of 50000 fps, as will be demonstrated in the following paragraph.

The flow visualization technique employed and the camera used allows for acquisition of 16-bit grayscale images, where dark and light-coloured areas correspond to flow regions dominated by vapour and liquid, respectively. In fact, the colour scaling of the figures corresponds to the value of the vapour fraction, i.e. black or white colours are indicative of pure vapour or liquid, respectively. A typical, "raw" image as produced by the visualization method can be seen in the bottom row of Fig. 2, where the shadow of the needle is also visible at the left part of the figure. The cavitation cloud is clearly discernible as a dark shadow occupying a significant part of the nozzle hole cross-section with a clearly defined interface having its leading edge exactly at the location of the geometrical constriction. Furthermore, a coherent vapour structure can be clearly seen to have been detached from the main cloud cavity and being convected downstream by the main flow.

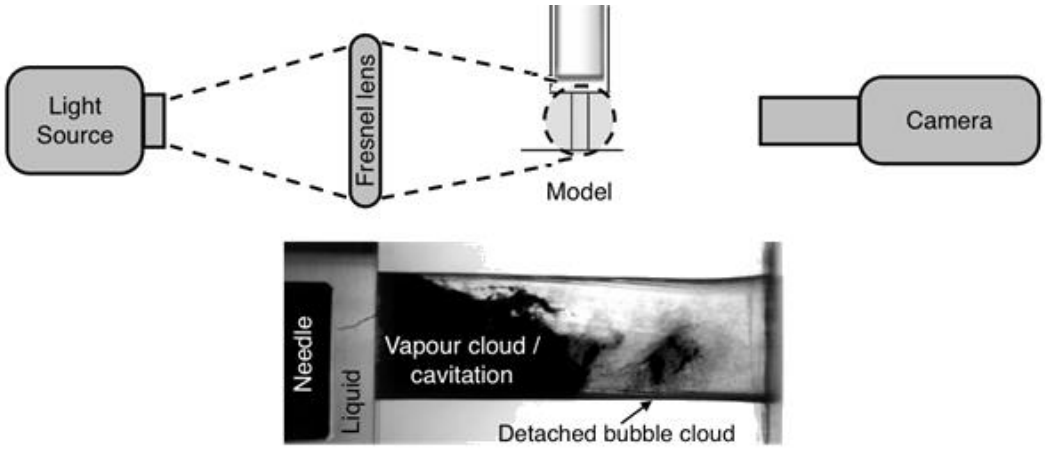

Figure 2. Top row: Shadowgraphy technique arrangement and bottom row: sample raw-data image of the cavitating flow inside the flow channel.

Since the collapse of coherent cavitating vortices has been linked to increased erosion aggression [30,35], accurate identification of the exact locations of vortex-cavitation inception and collapse is of high value when referring to injector nozzle flows. In order to be able to clearly identify a vapour cloud separation in the examined geometrical layout, initially, the grayscale range of the high-speed images was inverted (complimentary image), i.e. areas of pure vapour and liquid now corresponded to white and black-coloured pixels, respectively. A proper thresholding methodology was applied in order to detect only vapour pockets that totally refract light away of the camera and a threshold correction was imposed to lower the sensitivity of the detection method on clouds of low bubble density that produce mid-range grey pixel values. Hence, only well-established clouds that produce high brightness values were reproduced to the binarized (black and white) images that resulted after thresholding.

Graphs, having the typical form shown in Fig. 3 were produced by plotting the mean pixel brightness against the non-dimensional channel length. Indicative "raw", shadowgraphy images from which the mean-brightness images were produced, are also presented on the top part of Fig. 3. The average pixel-brightness values for each location along the hole length, resulted by averaging the brightness values (after the proper thresholding) of all the pixels along the entire nozzle diameter. In essence, the values of each line of the 512 x 208 matrix representing the spatial resolution of the visualization technique were averaged in order to produce each point of the curve shown in Fig. 3. A common feature that was detected in all graphs is a steep brightness increase until a peak is reached shorty downstream of the nozzle inlet, $L/L_0=0$, where L is the spatial co-ordinate along the flow direction and L_0 the overall injector-hole length. This trend is quite expected, as the nozzle region immediately downstream of the geometrical constriction imposed by the needle and needle seat is always occupied by vapour cloud regardless of the operating conditions.

However, additional local peaks could be discerned in the mean pixel-brightness graphs, as depicted in two different time-instances, b and c, of Fig. 3. These peaks could indicate the detachment of a coherent cavitating vortex and were monitored by the image-processing algorithm. According to this procedure, if a local maximum value of the pixel mean-brightness is detected downstream of a respective local minimum value, the image-processing algorithm is set to monitor this characteristic sequence. If the same pattern is encountered in a subsequent discretized segment of the nozzle length, i.e. at a further downstream location, as indicated by the square-marked region in red colour in the nozzle region between the non-dimensional lengths of 0.5 and 0.75 (see Fig. 3), then the original location, where the peak was initially observed, is recorded as a separation point.

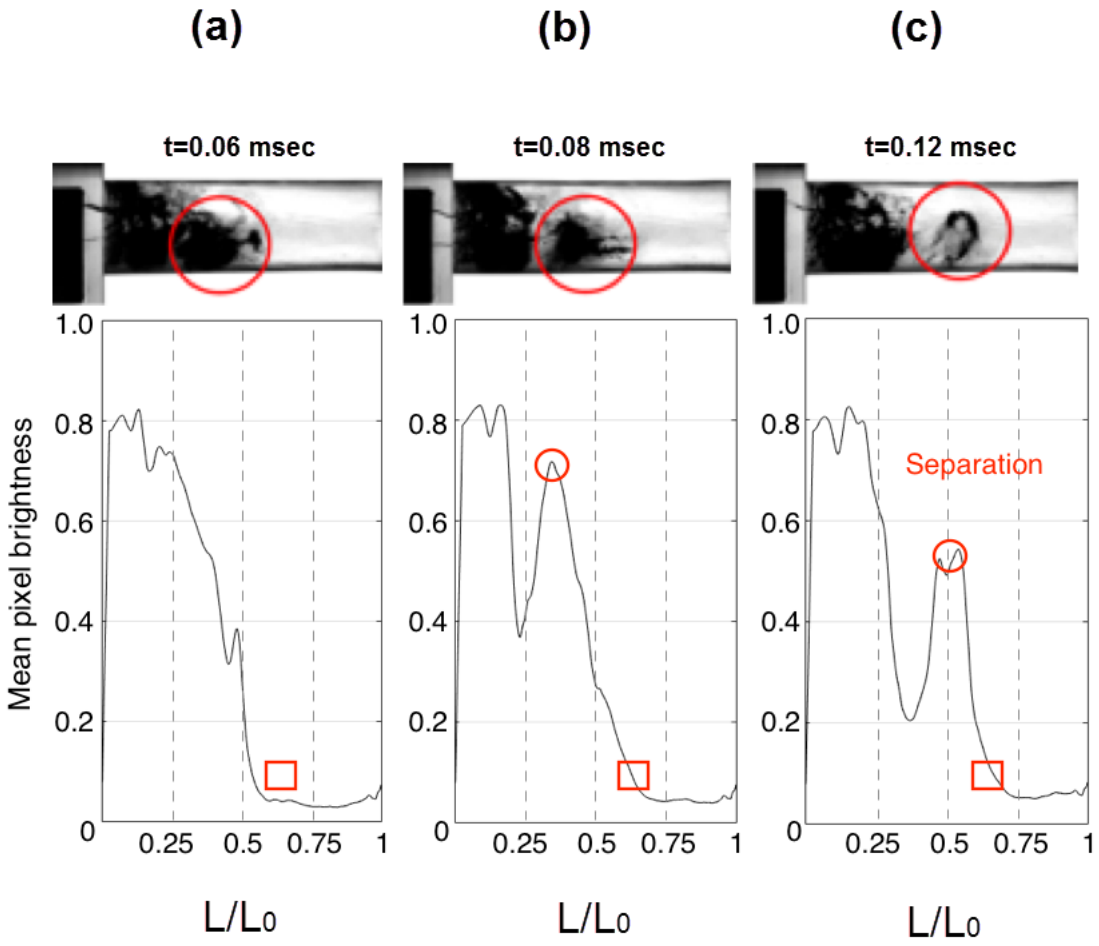

Figure 3. Procedure followed for the identification of a cavitating vortex detachment. The graphs present mean-pixel brightness inside the flow channel versus channel non-dimensional length for consecutive time steps a, b and c.

3. RESULTS

The main findings of the investigation are presented in this section. Initially, the complex two-phase flow phenomena are thoroughly discussed and the underlying mechanisms responsible for their onset are identified. In a second stage, the influence of the main operating parameters such as the needle lift, as well as the cavitation and Reynolds numbers on the temporal and spatial development of the cavitation cloud are quantified. Finally, the extent of cavitation-induced erosion is characterized through x-ray tomography, of the nozzle surface wall deformation.

3.1 FLOW VISUALIZATION

A sequence of high-speed images depicting a typical periodical cycle of the formation and development of cloud cavitation in the injector hole is presented in **Fig. 4**. As has already been discussed, the effect of operating conditions on the temporal and spatial development of flow phenomena is also examined in this work, however the cloud topology illustrated in **Fig. 4** can

be considered as representative for all the cases examined. The overall duration of the flow event depicted is 0.16 ms. The first frame corresponding to the initiation of the characteristic flow event (t=0.0 ms) clearly depicts a vapour cloud, which develops immediately downstream of the geometrical constriction realized by the needle and the needle seat, appearing to occupy the entire nozzle cross-section. It is essential to indicate that the majority of the flow enters the nozzle hole from its lower half cross-section, since access to the respective upper part is restricted due to the asymmetrical layout of the needle. Although, cavitation still initiates around the complete periphery of the hole entrance edge, the varying flow conditions around the hole entry (due to restriction/asymmetry) cause the vapour cloud to either collapse at a short length downstream the entry, or to extend to longer lengths inside the injection hole. In fact, an additional flow visualization and quantification investigation regarding the present layout that has been performed employing micro-computed tomography [36] has demonstrated that the cavity, which remains attached around the periphery of the injector-nozzle entrance forms a ring-shaped (hollow) cavitation vapour pocket at the upper half of the hole cross-section. On the contrary, the lower half of the cross section is entirely filled with vapour; the cloud cavity extends further inside the hole, grows in size (volume) and provides the cavitation bubbles realizing by this way the detached vortical structures that are being shed.

The smooth, well-defined cloud interface discernible on the image referring to t=0.0 ms, transits to a highly unstable topology at t=0.02ms, where break up of small bubble clouds takes place almost on the entire extent of the cloud trailing edge. Since boundary-layer separation is a necessary condition for the emergence of cavitation in the vicinity of a solid wall, it is expected low pressure to prevail at the core of the recirculating flow that sets in near the nozzle inlet, while the pressure at the outer main flow is higher. The instability of the closure region is closely linked to the occurrence of this adverse pressure gradient, as liquid is drawn toward the wall surface and a stagnation point is formed. In addition, the existence of the adverse pressure gradient leads to liquid flowing toward the flow-separated region, i.e. opposite to the main flow. This liquid upstream motion corresponds to the well-established mechanism commonly termed as re-entrant jet.

Already at t=0.04 ms the cloud has reached its maximum length. The outer region of the cavity appears to have been detached from the nozzle wall and a stream of liquid, which is in fact the re-entrant jet, flows beneath it, as indicated in the respective time instance of Fig. 4. A rupture of the vapour pocket can also be detected, denoted as a light coloured region in the cavity core protruding from the nozzle wall, which is attributed to the impingement of the re-entrant jet on the attached recirculating flow causing the local collapse of bubbles. The detachment of the coherent vapour structure commences exactly from this region, as the re-entrant jet turns upwards and severs the attached cavity. As shown on the frame captured at t=0.06 ms, a coherent vapour structure has been completely cut off from the attached cavity. The detached vapour cloud is convected downstream by the main flow as shown on the frames corresponding to t=0.08 ms and t=0.10 ms. As stated by Gopalan and Katz [17] the collapse of vapour bubbles is responsible for increased vorticity in regions of recirculating flow, while the presence of bubbles in the core of a vortex has also been identified as a cause for increased vorticity magnitude[16]. Thus, the detached cloud cavity is postulated as a large-scale vortex carrying bubbles, which initially emanated at the region of the attached cavity. It is important to point out that the curvature of the nozzle wall facilitates the formation of a three-dimensional separated vortical structure, similar to that detected in the case of a twisted hydrofoil [37], due to the radially diverging re-entrant jet collision with the three-dimensional interface of the attached cavity.

The relatively round initial shape of the detached cavitating vortex appears to shrink as higher pressure is encountered, e.g. as seen in frames corresponding to t=0.08 ms and t=0.10 ms, while it obtains a relatively arbitral shape in the first moments following its emanation.

The vortex topology tilts to the front possibly due to the difference in the mean flow velocity magnitude between the boundary-layer region and the channel core. A fully three-dimensional, hairpin-shaped vortex carrying vapour bubbles in its core can be clearly detected at t=0.12ms having its right ligament leaning against the nozzle surface. The hairpin-shaped vapour cloud is entrained by the main flow until it collapses in a region of elevated pressure.

The two final frames of Fig. 4, corresponding to the final stages of the flow-event cycle clearly illustrate that the cavitating vortex loses its coherence as it travels with the main flow. The vortex ligaments are separated at t=0.14 ms, while the upper ligament seems to have broken up almost entirely at t=0.16ms due to viscous decay and pressure recovery. It is noteworthy to mention that the lower vortex ligament collapses in the vicinity of the nozzle wall and, thus, the specific region is expected to exhibit significant cavitation-induced erosion. Although the images shown in Fig. 4 refer to a specific test case, the formation of the vapour cloud, as well as the shedding of cavitation vortices are consistent observations made regardless of the operating conditions and the needle lift. It should also be noted that, in general, the two-phase flow is highly unstable almost in the entire hole cross-section. For example, string-like cavitation structures are evident to develop and collapse on the upper nozzle half cross-section, e.g. as seen in frames taken at t=0.02 ms and t=0.04 ms. However, their importance in terms of cavitation erosion is negligible, since their collapse occurs away from the wall surface.

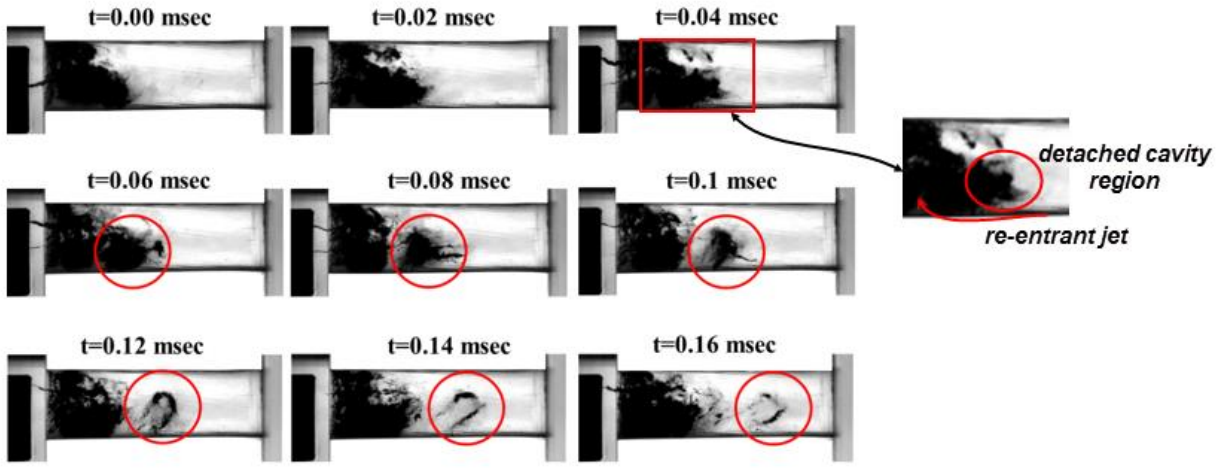

Figure 4. Sequence of flow events referring to a case characterized by Lift = 0.5mm, CN = 1.3 and Re = 53760 (Case Id. L0.5_CN1.3_L).

3.2 POST-PROCESSING RESULTS

The influence of the prevailing flow conditions on the dynamic flow features is presented in this section. In a first step, the influence of the cavitation number on the temporal evolution of vortex-cavitation shedding is examined. It is essential to clarify that, based on the current definition of the cavitation number, higher values correspond to a more established cavity pocket downstream of the geometrical constriction. The Strouhal number *(=fL/u)* was employed as a quantity representative of the shedding frequency *f*. Initially, the shedding time period was measured as the time interval between the complete detachments of two consecutive vortical clouds. Consequently, the frequency was calculated as the inverse of the aforementioned time period. The nozzle length *L* and the average flow velocity *u* in the injector hole, calculated by the imposed flow rate and the nozzle cross-section, were selected as the characteristic length velocity and scales also required for the definition of St. The Strouhal number values shown in Figs. 5-7 correspond to characteristic time periods of the periodical phenomenon in the range 0.04ms-3.82ms with 0.02 ms time intervals in-between (as designated

by the frame rate of 50000 fps). Therefore, the respective frequencies lie in the range 262-25000 Hz, with the maximum frequency presented being limited to half of the camera frame rate. The uncertainty associated with the Strouhal number values was calculated considering the error propagation, as described by Moffat [33], due to the uncertainty in the measured values regarding frequency, velocity and nozzle length. The uncertainty in the Strouhal number values in the range 1-5, which is of interest, results in the range 3.3%-4.1%.

Figs. 5-7, in essence, illustrates the probability of a vortex-shedding cycle, i.e. the detachment of consecutive cavitating vortices, to occur with a characteristic frequency corresponding to a specified value of the Strouhal number. The probability values have been considered not to be associated with uncertainty, since each frame, where the characteristic brightness pattern corresponding to a separation appears, is recorded according to the procedure also mentioned in paragraph 2. Consequently, the occurrence probability results as the percentage of the frames where a separation is identified compared to all the frames recorded. Referring to Fig. 5, for the lowest value of the cavitation number (CN=1.4), a plateau can be discerned in the Strouhal-number ($St=fL/u$) values ranging from 2.0 to 3.1, whereas the probability of a cloud separation to occur with each frequency is relatively low and approximately equal to 10%. Hence, the vortex shedding does not justify a clear periodical behavior, since a dominant shedding frequency (i.e. Strouhal number) does not exist. It must be noted that the Strouhal-number values must be treated as nominal, since they have been defined in terms of an average velocity within the nozzle determined by the imposed flow rate. However, the flow velocity at the contraction region could be significantly higher. On the contrary, the flow shows a clear periodical behavior, as the cavitation number increases. The peak probability corresponding to 33% of the recorded cycles can be clearly detected for a value of the Strouhal number approximately equal to 5. The magnified view of the probability values for St<1, shown as inset on Fig. 5 elucidates that the detachment probability rapidly drops to zero for CN≥1.8, whereas for lower CN values it retains low values of the order of 0.5-5.0% for a wide range of St numbers, a trend that also justifies that the phenomenon becomes more chaotic as CN decreases. Besides, the detachment probability for CN=1.6, 1.8 and 2.0 obtains similar values for Strouhal-number values of the order of 1, exactly due to the aforementioned vortex-shedding behaviour. It has been verified that the accumulated probability of cavity-cloud detachment in the Strouhal-number range 0.1-5.0 is approximately equal to 100% and, thus, there cannot be a peak at higher, non-detectable Strouhal-number values. This leads to the deduction that the dominant frequency of the phenomenon corresponding to the maximum St that can be measured is well captured.

As has already been explained, the periodicity of the phenomenon is primarily influenced by the intensity of the re-entrant jet, which in turn is designated by the cavitation regime (sheet-cloud) and the geometrical layout. The attached cavity is better established for larger cavitation numbers; thus, the adverse pressure gradient in the separated boundary layer becomes steeper and the momentum of the re-entrant jet higher. Since the cloud detachment occurs due to the interaction of the jet with the interface of the attached cavity pocket, the presence of a jet of higher magnitude in the shear layer constitutes the complete separation of a vapour cloud much more plausible. In addition, the presence of more vapour bubbles enhances the boundary-layer vorticity, further enabling the separated cloud to roll up into a coherent vortical structure [16]. It is interesting to notice that the Strouhal-number values characterizing the shedding in the specific nozzle layout are considerably higher than the typical values detected in vortex shedding from hydrofoils, which is in the order of 0.2-0.3 [9]. The cause must be attributed to the different cavitation regime, as cloud cavitation prevails, instead of attached sheet cavitation typically occurring in hydrofoils. Besides, it has been shown by Pelz et al. [32] for a wedge configuration that the Strouhal number obtains much higher values, when referring to cloud compared to the sheet cavitation regime.

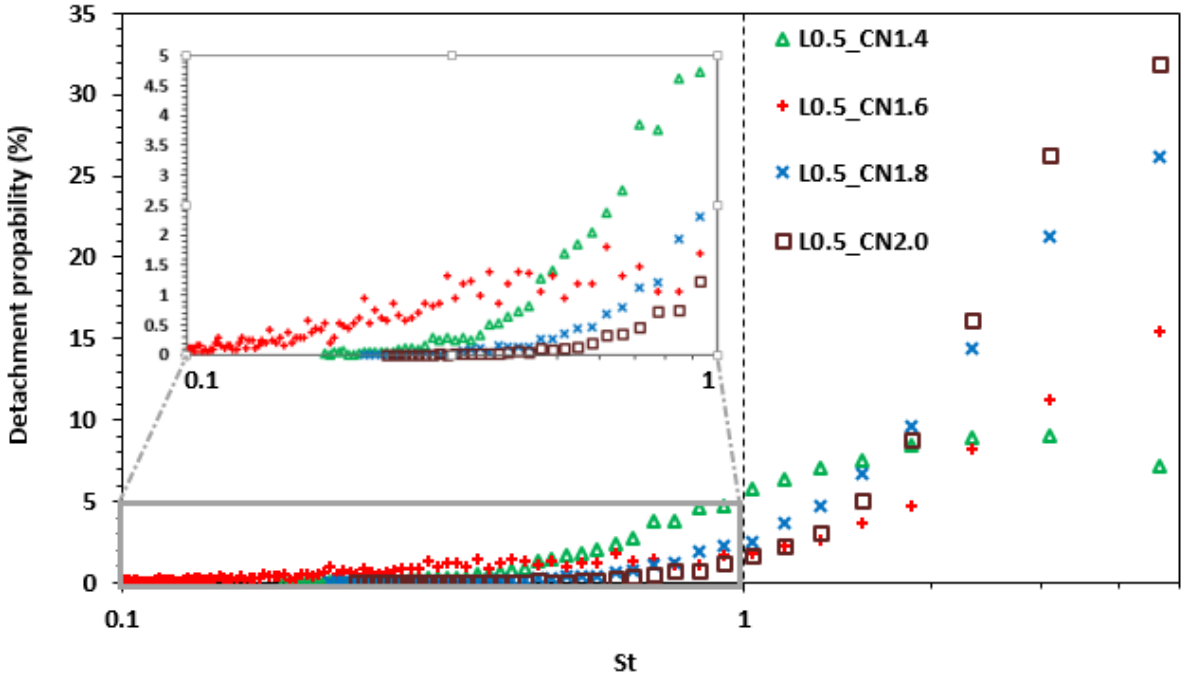

Figure 5. Effect of the cavitation number CN on the temporal evolution of cavitation-vortex shedding for Re=53760 and needle lift equal to 0.5mm.

The effect of the Reynolds number on the shedding frequency of the cavitating hairpin vortices is illustrated in Fig. 6, considering the cavitation number as an additional influencing parameter. Referring to CN=1.3, a single prevailing shedding frequency can be detected, which corresponds to a Strouhal number approximately equal to 3.1 for the lower value of the Reynolds number considered (Re=53760). The vortex-shedding frequency increases with the Reynolds number up to the maximum detectable Strouhal-number value approximately equal to 5.0, while the periodicity of the phenomenon is slightly enhanced since the percentage of vortical structures recorded being shed with the frequency of maximum detectable probability is higher compared to Re=53760 (18% instead of 15%). It must be mentioned that in the test case characterized by CN=1.3 and Re=63663, the accumulated shedding probability with a Strouhal number in the range 0.1-5.0 is equal to 73%. Hence, the evolution of the phenomenon could be even more rapid, i.e. there is a 27% probability corresponding to additional shedding frequencies characterized by Strouhal-number values higher than 5.0, which exceed the temporal resolution of the visualization technique. The inducement of more rapid vortex shedding is justified, as higher flow velocity leads to a more significant separation downstream of the contraction realized by the needle and needle seat and hence increased levels of vorticity in the boundary-layer region, as well as a steeper adverse pressure gradient producing a re-entrant jet of higher momentum, which reaches the interface of the cavity attached on the nozzle wall in a shorter time period and causes a more frequent detachment of a vapour cloud.

The manifestation of the shedding mechanism in a periodical manner is clearly enhanced with increase of the Reynolds number for a higher cavitation-number value considered equal to 1.45, as also shown in Fig. 6. It is interesting to notice that the peak-probability Strouhal number for a specific Reynolds number actually decreases slightly compared to the respective for CN=1.3. In other words, increase of the main flow-velocity seems to favour the cavitating vortices being shed with the lower frequency. This flow behavior, although counter-intuitive, is in agreement with the observations of Gavaises et al. [20], which reported that increase of the Reynolds number leads to a shedding sequence of lower frequency due to the agglomeration

of vortex cavities that live longer due to the increased cavitation number. It must also be mentioned that, for CN=1.45, the accumulated probability the shedding to be manifested with a Strouhal number lying in the range 0.1-5.0 is equal to 85%. Since the peak probability detected within the measuring range is in the order of 22%, a probability plateau for Strouhal-number values larger than 3.1 is possible to occur if a single peak of 15% exists for St>5.0, namely outside the detectable range. In any other case the dominant frequency corresponds to St=3.1.

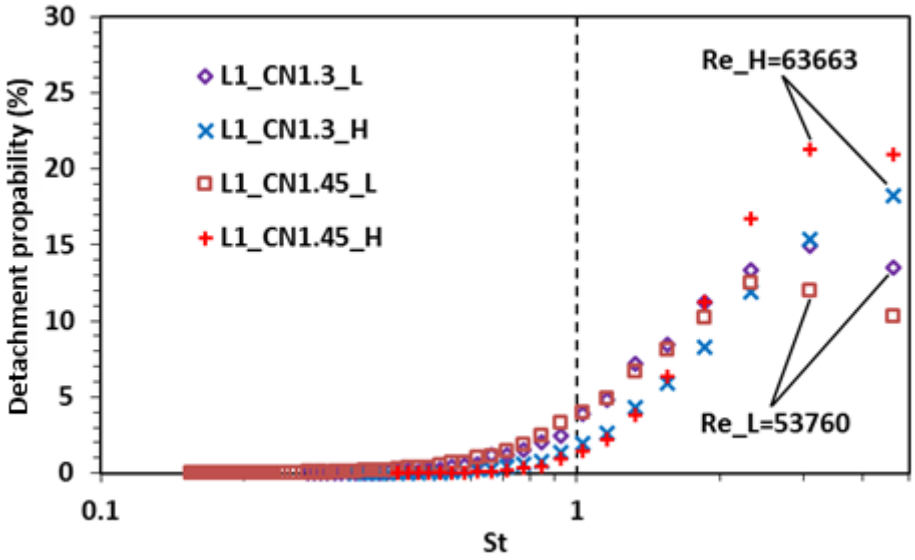

Figure 6. Effect of the main-flow Reynolds number on the temporal evolution of cavitation-vortex shedding for different cavitation-number values and needle lift equal to 1.0 mm.

Fig. 7 elucidates the influence of the needle lift on the dynamical evolution of vortical cavitation. As it is clearly illustrated, increase of the relative position of the needle in reference to the injection-hole entry from 0.5 to 2.0 mm enhances the periodicity of vortex shedding. The prevailing shedding frequency remains constant and corresponds to a Strouhal value of 3.1 for needle lifts equal to 1.0 and 2.0 mm, respectively, whereas a characteristic frequency cannot be detected for a lift equal to 0.5 mm. This trend can be justified by taking into account that the flow passage becomes narrower as the needle lift decreases (throttling effect). Hence, the flow experiences a more significant blockage prior to entering the nozzle and, subsequently, a more severe expansion within the injection hole. The body of the needle, in essence, acts as an obstacle, which provokes further instability in the already highly turbulent flow. The flow separation downstream of the abrupt geometrical contraction becomes more violent due to the steeper adverse pressure gradient occurring in the contraction region and the sequence of vortex shedding becomes more stochastic. The probability of shedding occurrence with frequencies up to 25.0kHz, i.e. St≈5.0, is in the order of 96.5%, 88.5% and 90.5% for needle lifts of 0.5, 1.0 and 2.0mm, while the probability peaks detected for these cases are approximately equal to to 10%, 15% and 20%, respectively. It can be therefore justified that the clear peak-probability frequencies existing for lifts of 1.0 and 2.0mm within the detectable range are in fact the dominant ones.

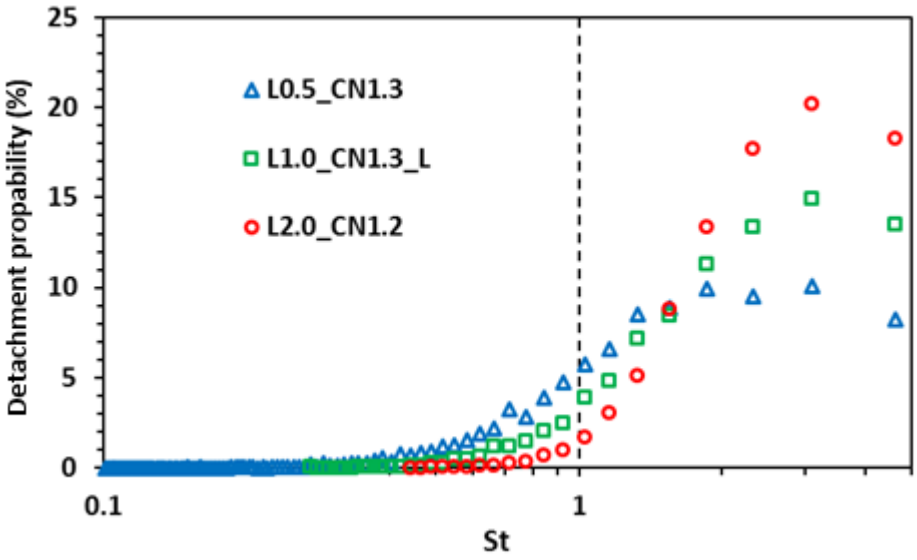

Figure 7. Effect of the needle lift on the temporal evolution of cavitation-vortex shedding for Re=53760.

It is of high engineering value to be able to accurately pinpoint the locations where vortical-cavitation structures collapse, as these sites qualify as possible erosion sites. The three following figures give insight on the impact of the prevailing flow conditions on the life period and the spatial development of the cavitating vortices that have been found to emerge within the injector nozzle. Figs. 8-10, in essence, illustrate the probability a detached vortical structure to collapse at a specified location along the injector-hole length. Initially the effect of the cavitation number is considered and, as can be seen in Fig. 8, increased values of the specific quantity lead to the onset of hairpin vortices that travel longer with the main flow and collapse at locations closer to the nozzle outlet. The vast majority of vortices recorded for the lowest value of the cavitation number (CN=0.9) collapse prior to the nozzle mid-length, with a probability peak at a location corresponding to a third of the total length. On the other hand, for CN=1.45 most of the cavitating vortices recorded collapse at a location close to 0.8 of the channel length. This trend is in compliance with the conclusions mentioned in the discussion of Fig. 5. A larger cavitation number is indicative of increased intensity of the cavity pocket, as well as increased vorticity in the flow-separation region. Hence, the effect of the cavitation number on the location where vortex cavitation collapses, in essence, also describes the corresponding effect of the vapor cloud length. As CN increases from 0.9 to 1.3, the vortices detaching from the attached cavity trailing edge, which is, in fact, closer to the hole outlet due to the larger extent of the cavity pocket, travel longer with the main flow due to their increased vorticity magnitude and surplus of vapour bubbles and collapse at locations close to the nozzle outlet ($L/L_0 \approx 0.8$). However, it must be noted that increase of the cavitation number from 1.3 to 1.45 does not alter the location, where the peak value of collapses occurs. This must be attributed to the upstream effect of the outlet, which induces flow instabilities that cause the vortex collapse.

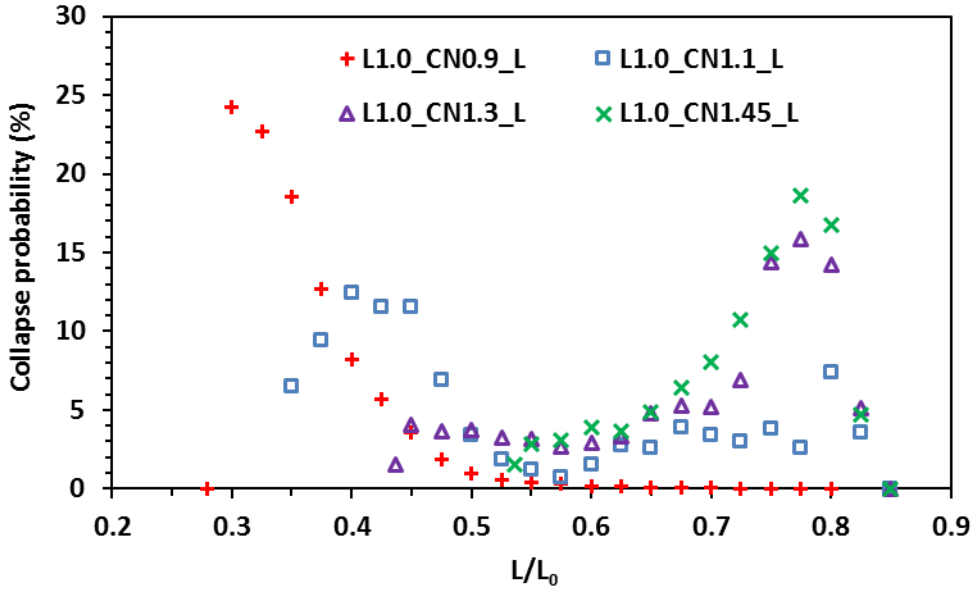

Figure 8. Effect of cavitation number CN on the location of vortex-cavitation collapse for Re=53760 and needle lift equal to 1.0 mm.

As elucidated by Fig. 4, the main flow is responsible for entraining the cavitating vortices downstream of the site of their onset and consequently its velocity magnitude could have a significant influence on the life period of the detached cavities and the location of their collapse. Fig. 9 shows that for a cavitation number of 1.3 the location closest to the nozzle inlet, where probability of vapour collapse has been detected, is shifted from slightly upstream of 0.45 to 0.55 of the hole length, indicating that the coherent vortices are, in general, traveling longer with the main flow, as the Reynolds number increases from 53760 to 63663. Nevertheless, it is clearly discernible in the graph of Fig. 9 corresponding to CN=1.3, that the location of maximum vortex-collapse probability for Re=53760 ($L/L_0 \approx 0.76$) is closer to the nozzle outlet in comparison to the respective for Re=63663 ($L/L_0 \approx 0.70$). Although, the underlying cause of this distinct flow behavior, which seems to mainly have an influence on the vortices shed with the dominant frequency, is not utterly clear, it could be attributed to the fact that the main flow affects the vortex development, as it tilts its topology (see also Fig. 4). Since the cavitation number is not high, the moderate magnitude of the vortical cavities could be affected in a hindering manner by the higher momentum of the main flow, which could exhibit a tendency to push the structures closer to the nozzle wall, hence leading to a shorter time period.

Besides, it is interesting to notice that, for CN=1.3 and Re=63663, a local maximum of the collapse probability can be discerned at $L/L_0=0.55$. In accordance to the discussion referring to Fig. 6 for the aforementioned flow conditions, the shedding sequence is very rapid and it is possible the limitation imposed by the camera frame rate to constitute the visualization of the dominant frequency infeasible. The fact that both a local and a global maximum value of vapour-collapse probability can be detected on Fig. 9 for CN=1.3, can only be indicative of more than one shedding frequencies with high probability. As depicted on Fig. 6, both Strouhal number values of 3.1 and 5.0 exhibit high occurrence probabilities and hence the two distinct collapse locations could be corresponding to the shedding sequences characterized by these frequencies.

On the contrary, the impact of the main-flow velocity on the life period of the vortical cavities appears to be non-significant for CN=1.45, as the structures exhibit a specific collapse pattern regardless of the Reynolds number. Moderately higher probability values of vapour collapse are encountered toward locations closer to the injector-hole outlet for Re=63663, however, the maximum probability is in the order of 20% in both cases corresponding to

slightly different locations close to 0.8 of the nozzle length. For CN=1.45, the vortices are postulated to have a well-established topology and considerable magnitude allowing them to travel up to around 80% of the injector length, where flow instabilities caused by the presence of the outlet lead to their decay.

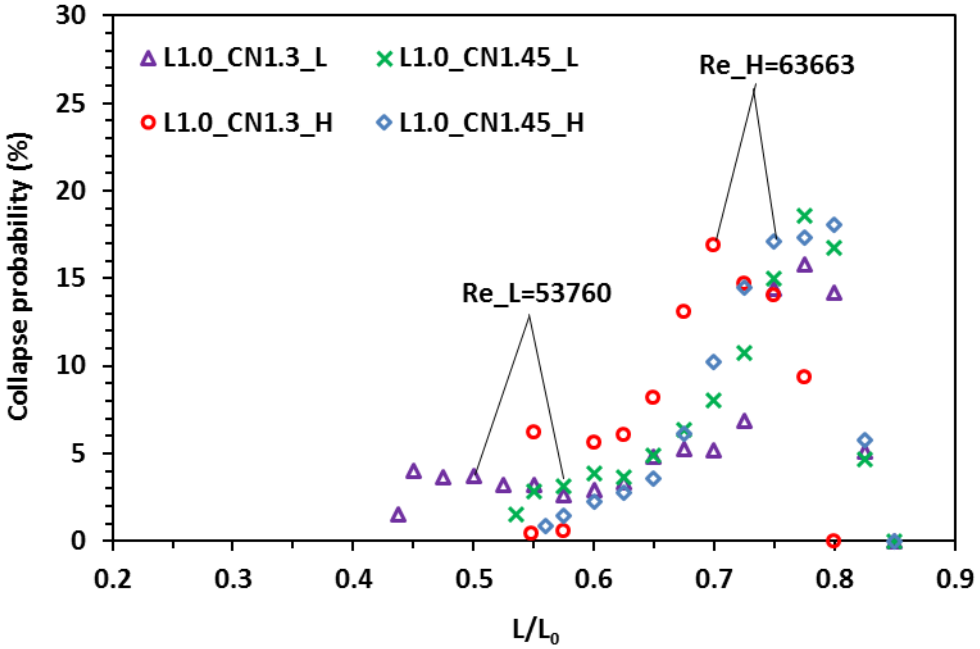

Figure 9. Effect of the Reynolds number on the location of vortex-cavitation collapse for different cavitation numbers and needle lift equal to 1.0 mm.

The flow-passage layout is expected to have a considerable impact on the topology of vortical cavitation, since it acts as a controlling parameter for the intensity of both the flow separation downstream of the geometrical contraction and the extent of the cavity pocket developing within the nozzle. The effect of the needle lift on the life period of the cavitating vortices is shown in Fig. 10, where the cavitation number is also considered as a parameter. In reference to the lower cavitation number (CN=1.0), increasing the needle lift from 1.0 to 2.0mm, clearly enhances the magnitude of the vapour vortices, since all the structures recorded collapse at 0.34 of the nozzle length or downstream of that location, whereas in the case of 1.0 mm lift, almost 64% of the recorded vortices have collapsed at locations closer to the hole inlet. Besides, the peak value in the graph (at L/L_0=0.34) indicating the location at which the vortex-cavities are most likely to collapse, is more profound in the case of 2.0 mm lift, supporting the conclusion drawn in the discussion referring to Fig. 7, that a wider gap between the needle and the needle seat enhances the periodical nature of the vortex-shedding sequence. It has been made clear that the transient structures emerging inside the injector for low values of the cavitation number and needle lift higher than 1.0 mm, are characterized by a single prevailing onset frequency and have a characteristic life span associated with a high-probability location of vapour collapse.

On the contrary, for CN=1.2, the spatial evolution of the flow phenomena seems to be relatively insensitive to the needle lift, as for increased lift, the pattern of locations, where the detached vapour clouds collapse, exhibits an almost negligible shift toward the nozzle outlet. Besides, the region where vapour collapse has been recorded exhibits a higher scattering compared to the lower cavitation number, spanning along 0.35 to 0.8 of the overall nozzle length. It is also interesting to observe that the most probable location of the hairpin-vortex collapse is detected in the range 0.74-0.78 of the nozzle length, while there is an additional, local maximum value of collapse probability approximately at 0.42. As illustrated by Fig. 7 for

values of the cavitation number equal to 1.2 or higher and needle lift in the range 0.5-2.0mm additional frequencies apart from the prevailing one obtain high probability values. Thus, a considerable number of shedding cavities of different yet distinct life span set in, which subsequently collapse at different locations. It can therefore be justified that the cavitation number has a much more considerable impact on the spatial development of vortical cavitation, rather than the geometrical contraction of the flow passage.

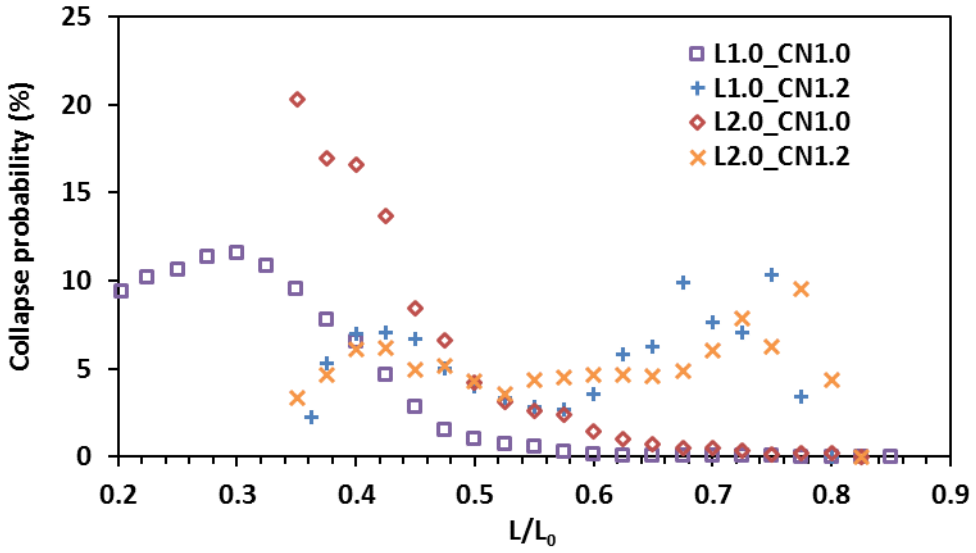

Figure 10. Effect of needle lift on vortex-cavitation collapse for different values of the cavitation number.

4. CONCLUSIONS

The present study provides insight on the highly transient, cavitating-flow topology that develops inside an enlarged, single-hole, transparent replica of a fuel-injector nozzle by means of high-speed shadowgraphy imaging. The manifestation of a periodical vortex-shedding sequence within the injector nozzle has been verified. Coherent, cavitating vortical structures have been illustrated to detach from the attached cloud cavity that establishes in the vicinity of the nozzle inlet due to the action of the physical mechanism, commonly termed as re-entrant jet. The vortices, which act as carriers of vapour bubbles, are entrained by the main flow to downstream nozzle locations and obtain a characteristic hairpin-like shape prior to the decay of their coherence and their eventual collapse. A wide range of operating scenarios were examined, so as to clarify the influence of the main flow parameters, i.e. Re, CN and needle lift on the temporal and spatial characteristics of the detached cavitating vortices. It has been established that increase of either the cavitation number or of the gap between the needle and needle seat, leads to a clear enhancement of the shedding-sequence periodical nature, without affecting its dominant frequency. Increase of the main-flow Reynolds number for a specific cavitation-number value has also been found to enhance the phenomenon periodicity.

In a second step, the life period and the spatial evolution of the emerging cavitating vortices has been characterized with special focus given to the location of their collapse. Increase of the cavitation number was found to have a clear beneficial effect on the life period of the detached vortex cavities. On the contrary, it was established that the value of the Reynolds number characterizing the main flow had a non-significant influence on the spatial development of vortex-cavitation. The impact of the needle lift was considerable for the lower cavitation number examined (CN=1.0), as increase of the lift lead to a clear shift of collapse probability

toward locations farther from the nozzle inlet. However, for a higher cavitation number considered (CN=1.2) the needle-lift effect was significantly mitigated.

ACKNOWLEDGMENTS

The research leading to these results has received funding from the People Programme (IOF Marie Curie Actions) of the European Union's Seventh Framework Programme FP7/2007-2013/ under REA grant agreements n. 300410 and n. 324313.

REFERENCES

[1] O. Griffin, "Bodies in a Shear Flow: A Review," J. Fluids Eng. **107**, 298 (1985).

[2] P. Ausoni, M. Farhat, X. Escaler, E. Egusquiza, and F. Avellan, "Cavitation Influence on von Kármán Vortex Shedding and Induced Hydrofoil Vibrations," J. Fluids Eng. **129**, 966 (2007).

[3] B. Ji, X. Luo, R. E. A. Arndt, and Y. Wu, "Numerical simulation of three dimensional cavitation shedding dynamics with special emphasis on cavitation–vortex interaction," Ocean Eng. **87**, 64 (2014).

[4] R. E. A. Arndt and A. P. Keller, "Water Quality Effects on Cavitation Inception in a Trailing Vortex," J. Fluids Eng. **114**, 430 (1992).

[5] R. E. A. Arndt, "Cavitation in Vortical Flows," Annu. Rev. Fluid Mech. **34**, 143 (2002).

[6] G. H. Schnerr, I. H. Sezal, and S. J. Schmidt, "Numerical investigation of three-dimensional cloud cavitation with special emphasis on collapse induced shock dynamics," Phys. Fluids **20**, 040703 (2008).

[7]K. R. Laberteaux, S. L. Ceccio, V. J. Mastrocola, and J. L. Lowrance, "High speed digital imaging of cavitating vortices," Exp. Fluids **24**, 489 (1998).

[8] Y. Kawanami, H. Kato, H. Yamaguchi, M. Tanimura, and Y. Tagaya, "Mechanism and Control of Cloud Cavitation," J. Fluids Eng. **119**, 788 (1997).

[9] M. Kjeldsen, R. E. A Arndt, and M. Effertz, "Spectral Characteristics of Sheet / Cloud Cavitation," J. Fluids Eng. **122**, 481 (2000).

[10] A. Kubota, H. Kato, and H. Yamaguchi, "A new modelling of cavitating flows: a numerical study of unsteady cavitation on a hydrofoil section," J. Fluid Mech. **240**, 59 (1992).

[11] G. Wang and M. Ostoja-Starzewski, "Large eddy simulation of a sheet/cloud cavitation on a NACA0015 hydrofoil," Appl. Math. Model. **31**, 417 (2007).

[12] B. Huang, Y. Zhao, and G. Wang, "Large Eddy Simulation of turbulent vortex-cavitation interactions in transient sheet/cloud cavitating flows," Comput. Fluids **92**, 113–124 (2014).

[13] Q. Qin, C. C. S. Song, and R. E. A. Arndt, "A numerical study of an unsteady turbulent wake behind a cavitating hydrofoil," *Proceedings of the Fifth Int. Symp. Cavitation*, Osaka, Japan, 1-4 November 2003.

[14] E. J. Foeth, C. W. H. Van Doorne, T. Van Terwisga, and B. Wieneke, "Time resolved PIV and flow visualization of 3D sheet cavitation," Exp. Fluids **40**, 503 (2006).

[15] R. E. A. Arndt, V. H. Arakeri, and H. Higuchi, "Some observations of tip-vortex cavitation," J. Fluid Mech. **229,** 269 (1991).

[16]G. Sridhar and J. Katz, "Effect of entrained bubbles on the structure of vortex rings," J. Fluid Mech. **397**, 171 (2000).

[17] S. Gopalan and J. Katz, "Flow structure and modeling issues in the closure region of attached cavitation," Phys. Fluids **12**, 895 (2000).

[18] H. Ganesh, S. A. Mäkiharju, and S. L. Ceccio, "Interaction of a Compressible Bubbly Flow With an Obstacle Placed Within a Shedding Partial Cavity," J. Phys. Conf. Ser. **656**, 012151 (2015).

[19] B. Stutz and S. Legoupil, "X-ray measurements within unsteady cavitation," Exp. Fluids **35**, 130 (2003).

[20] M. Gavaises, F. Villa, P. Koukouvinis, M. Marengo, and J. P. Franc, "Visualization and les simulation of cavitation cloud formation and collapse in an axisymmetric geometry," Int. J. Multiph. Flow **68**, 14 (2015).

[21] A. Andriotis, and M. Gavaises, "Influence of vortex flow and cavitation on near-nozzle diesel spray dispersion angle," Atom. Sprays **19**, 247 (2009).

[22] N. Mitroglou, M. Gavaises, J. M. Nouri and C. Arcoumanis, "Cavitation inside enlarged and real-size fully transparent injector nozzles and its effect on near nozzle spray formation," *Proceedings of the Droplet Impact Phenomena and Spray Investigations Workshop 2011*, Bergamo, Italy, 27 May 2011.

[23] M. Gavaises, A. Andriotis, D. Papoulias, N. Mitroglou, and A. Theodorakakos, "Characterization of string cavitation in large-scale Diesel nozzles with tapered holes," Phys. Fluids **21**, 052107 (2009).

[24] A. Andriotis, M. Gavaises, and C. Arcoumanis, "Vortex flow and cavitation in diesel injector nozzles," J. Fluid Mech **610**, 195 (2008).

[25] E. Giannadakis, M. Gavaises, and C. Arcoumanis, "Modelling of cavitation in diesel injector nozzles," J. Fluid Mech **616**, 153 (2008).

[26] N. Mitroglou and M. Gavaises, "Mapping of cavitating flow regimes in injectors for medium-/heavy-duty diesel engines," Int. J. Engine Res. **14**, 590 (2013).

[27] N. Mitroglou, M. Lorenzi, M. Santini, M. Gavaises, and D. Assanis, "Application of cone-beam micro-CT on high-speed Diesel flows and quantitative cavitation measurements," J. Phys. Conf. Ser. **012094**, (2015).

[28] B. A. Reid, G. K. Hargrave, C. P. Garner, and G. Wigley, "An investigation of string cavitation in a true-scale fuel injector flow geometry at high pressure," Phys. Fluids **22**, 031703 (2010).

[29] B. A. Reid, M. Gavaises, N. Mitroglou, G. K. Hargrave, C. P. Garner, E. J. Long, and R. M. McDavid, "On the formation of string cavitation inside fuel injectors," Exp. Fluids **55**, 1661 (2014).

[30] M. Petkovšek and M. Dular, "Simultaneous observation of cavitation structures and cavitation erosion," Wear **300**, 55 (2013).

[31] M. Dular, B. Bachert, B. Stoffel, and B. Širok, "Relationship between cavitation structures and cavitation damage," Wear **257**, 1176 (2004).

[32] P.F. Pelz, T. Keil, G. Ludwig, in *Advanced Experimental and Numerical Techniques for Cavitation Erosion Prediction,* edited by K. H. Kim, G. Chahine, J. P. Franc, A. Karimi (Springer Verlag, Dordrecht, 2014) pp.221-237.

[33] R.J. Moffat, "Describing the uncertainties in experimental results," Exp. Therm. Fluid Sci. **1**, 3 (1988).

[34] N.I. Kolev, *Multiphase Flow Dynamics 3: Turbulence, Gas Absorption and Release, Diesel Fuel Properties,* Springer, Heidelberg, 2007.

[35] M. Dular and M. Petkovšek, "On the Mechanisms of Cavitation Erosion – Coupling High Speed Videos to Damage Patterns," Exp. Therm. Fluid Sci. **68**, 359 (2015).

[36] N. Mitroglou, M. Lorenzi, M. Santini, and M. Gavaises, "Application of X‐ray micro‐computed tomography on high‐speed cavitating diesel fuel flows", Exp. Fluids **57**, 175 (2016).

[37] B. Ji, X. Luo, Y. Wu, X. Peng, and Y. Duan, "Numerical analysis of unsteady cavitating turbulent flow and shedding horse-shoe vortex structure around a twisted hydrofoil," *Int. J. Multiph. Flow* **51**, 33 (2013).